Measurement of Flame Frequency Response Functions Under Exhaust Gas Recirculation Conditions

Joseph Ranalli and Don Ferguson

National Energy Technology Laboratory, Morgantown, WV 26507

Abstract

Background: Exhaust gas recirculation has been proposed as a potential strategy for reducing the cost and efficiency penalty associated with post-combustion carbon capture. However, this approach may cause as-yet unresolved effects on the combustion process, including additional potential for the occurrence of thermoacoustic instabilities. Method of Approach: Flame dynamics, characterized by the flame transfer function, were measured in traditional swirl stabilized and low-swirl injector combustor configurations, subject to exhaust gas circulation simulated by N_2 and CO_2 dilution. Results and Conclusions: The flame transfer functions exhibited behavior consistent with a low-pass filter and showed phase dominated by delay. Flame transfer function frequencies were nondimensionalized using Strouhal number to highlight the convective nature of this delay. Dilution was observed to influence the dynamics primarily through its role in changing the size of the flame, indicating that it plays a similar role in determining the dynamics as changes in the equivalence ratio. Notch-like features in the flame transfer function were shown to be related to interference behaviors associated with the convective nature of the flame response. Some similarities between the two stabilization configurations proved limiting and generalization of the physical behaviors will require additional investigation.

I. Introduction

Gas turbine systems for power generation face increasingly stringent environmental constraints. Recently, increased pressure has been due to the potential for regulation of greenhouse gas emissions, including carbon dioxide (CO_2), prompting the need for combustion strategies which may make carbon capture and storage (CCS) possible. Generally speaking, three main approaches have been proposed to meet this challenge, pre-combustion capture,

post-combustion capture and oxy-fuel combustion[1]. While each of these strategies has individual advantages and disadvantages in the long term, post-combustion capture uses sufficiently mature technologies to offer near-term, low risk application, including the potential to be retrofit onto existing systems. In post-combustion carbon capture strategies, exhaust gas is scrubbed of carbon dioxide through membrane separation, amine absorption or some similar technology.

This type of post-combustion carbon separation would be expected to incur additional capital cost as well as plant efficiency penalties. Several recent studies have indicated possible cost reductions through implementation of Exhaust Gas Recirculation (EGR) [2–4]. EGR involves displacement of a portion of the inlet air by conditioned exhaust stream gases. Recycle of product gases is already widely used in reciporicating engines for Nitric Oxide (NOx) control. Relative to post-combustion carbon capture, EGR increases the exhaust CO_2 concentration and thus increases the driving force for separation of carbon from the exhaust stream and reduces the work required for separation. In addition, EGR reduces the total flow rate of exhaust, reducing the size requirements (and hence, the economic cost) for the separation plant.

Implementation of EGR is not completely free of issues. Introduction of EGR produces a variable reactant composition that may impact the occurrence of undesirable combustion events such as blowoff and combustion dynamics [5]. These concerns are similar to those encountered in investigation of fuel-flexible turbines. Research is thus still needed to assess the impact of EGR on the combustion process. The present study addresses this need by measuring the influence of simulated EGR on flame dynamics through analysis of flame transfer functions in a laboratory combustor.

II. Background

Lean combustion, as commonly used in modern power generation turbine systems, produces an exhaust stream primarily consisting of CO_2, N_2, H_2O and O_2. This exhaust requires some conditioning prior to use for EGR. Water must be removed from the exhaust gas, and the exhaust flow must be cooled prior to reintroduction in the compressor, in order to maintain cycle efficiency[2], [3]. Exhaust gas recirculation for gas turbine systems has been demonstrated in a research setting by ElKady et. al. [5], who operated a model practical combustor up to EGR levels of 35%. Demonstrations involving a vitiated reactant stream have also been performed [6].

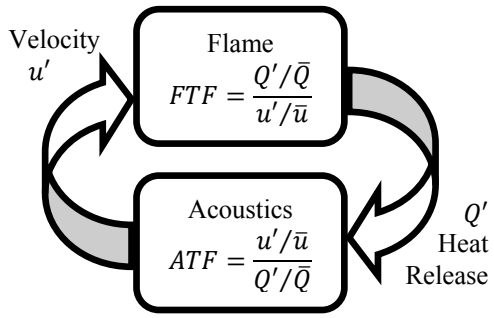

Fig. 1 - Sketch of closed-loop coupling process responsible for thermoacoustic instabilities. q' represents oscillations in the flame heat release rate and u' represents the acoustic velocity.

It is important to have an understanding of the influence of exhaust gas recirculation on the combustion process. Several prior studies have conducted investigation in this area, especially relative to emissions. ElKady et. al.[5] observe a 50% reduction in NOx production at 35% EGR level, though CO emissions are observed to increase slightly. Similar effects were observed by Røkke et. al. [7] and Evulet et. al. [6], due to flame temperature reductions and the larger reaction zone caused by dilution. Li et. al. [8] describe these effects in terms of EGR flames approaching a combustion regime more closely resembling a well-stirred reactor due to decreased flame speeds.

While general combustion issues have been investigated under EGR conditions, the effects of EGR on combustion dynamics remain relatively unknown. ElKady et. al. [5] describe a reduction in dynamic oscillations and attribute this behavior to changes in the heat release distribution zone. Ferguson et. al. [9], [10] observe that for both traditionally swirl stabilized and the low-swirl injector (LSI) [11] stabilized flames, EGR simulated by CO_2 and N_2 dilution causes changes in the dynamics that can be normalized by convective time delay. This effect can be said to be similar to dynamic changes resulting from other operating condition variations, such as equivalence ratio [9]. This convective normalization also highlights the importance of the heat release distribution in relation to the local velocity. They also observe that CO_2 has a greater impact than N_2. The present study provides measurements of flame transfer functions under EGR conditions to attempt to help investigate the cause of these dynamic observations found in literature.

Background on Thermoacoustic Instabilities

Thermoacoustic instabilities are the result of closed-loop coupling between the flame heat release rate and the system acoustics. A system level description of this behavior is shown in Fig. 1. Use of a system methodology for describing thermoacoustic interactions considers the flame and the acoustics to behave as independent transfer functions, each of which describe the frequency dependence of the response to a disturbance. The acoustic transfer function can be obtained through well-known means, either experimentally or via models. The flame transfer function, however, has been the subject of significant scrutiny.

The flame transfer function is most commonly described as the ratio of oscillations in the flame heat release rate (Q') to oscillations in the velocity (u'), normalized by their respective mean values, as follows:

$$FTF = \frac{Q'/\bar{Q}}{u'/\bar{u}} \tag{1}$$

Several investigations have focused on experimental [12–25] and theoretical [25–30] determinations of flame transfer functions. Common to many of these results is the observation that flame transfer functions exhibit a low-pass filter characteristic and obey a strong scaling relationship with the Strouhal number, a nondimensional frequency (f) measuring the ratio between convective and acoustic timescales:

$$St = f\frac{x_c}{u_c} \tag{2}$$

In this representation, x_c and u_c refer to a characteristic convective length and velocity respectively.

The effectiveness of this Strouhal number based formulation for flame transfer functions implies that interaction with convective disturbances plays an important role in the physics of flame-acoustic interaction. Several investigators (see for example [13], [14], [18], [20]) observe interactions between the flame and vortices convecting with the flow. This effect is also commonly considered in flame sheet modelling studies, which explicitly introduce forcing by such a disturbance [26–28]. Studies have also shown that this type of convective interation leads to interference which is associated with several features observed in the magnitude of the flame transfer function. This interference is both spatial in character and may result from the occurrence of multiple disturbances. For example, Palies et. al. show that portions of the flame can be shown to oscillate in- and out-of-phase in response to different excitation frequencies [13]. In addition to spatial interference, analysis contained in the same work also suggested the existence of an additional swirl perturbation that affected the flame angle, in addition to vortical disturbances. Another work by Palies et. al. considered the swirl perturbation in a theoretical framework and validated the approach with experimental data [25]. Experimental work by Jones et. al. [23] also observed the effect of multiple perturbations, one which they associated with flame anchoring and a second associated with shear layer vorticity disturbances. This effect is a common aspect of theoretical flame sheet models, which exhibit a flame-wrinkle response to acoustic excitation along with an explicitly introduced vortical disturbance [26–28]. O'Connor and Lieuwen [24], along with Acharya et. al. [30] also describe the impact of interference related to convective perturbations when considering transverse, rather than axial, acoustic excitations. A theoretical modelling effort by

the authors and coworkers attempts to provide a framework in which to distinguish the effects interference due to spatial effects and multiple perturbations based on convective analysis [29].

Significant variability exists in literature for the determination of the characteristic convective scales. Convective velocity is most commonly related to the mean flow velocity at the dump plane. Choice of characteristic length shows greater variability and has been related variously to: the axial distance to the maximum heat release rate (HRR) location, the inclined distance to the maximum HRR location from the centerbody, the axial distance to the flame "center of mass" (at times conflated with axial maximum HRR location) and the axial length of the flame. Confounding resolution of this inconsistency is the fact that the center of mass and peak HRR location are similar, and further, that the distance to the center of mass and the flame length are approximately proportional for a traditional swirl stabilized geometry [14] (termed HSI flames here). This proportionality allows nearly any of these choices for characteristic length to produce similar scalability according to Eq. 2. When dealing with flames in which this proportionality may not exist, such as lifted Low-Swirl Injector (LSI) flames [11], [31], no studies have attempted to identify the various governing scaling parameters.

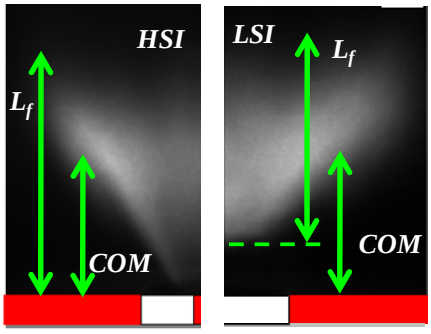

Fig. 2 – Sample images of flames for each injector type with the two applicable length scales notated. Note the different origin for base-to-tip flame length in the case of the LSI flame.

Modeling results by the authors and coworkers [29] suggest that the magnitude and phase of the flame transfer function are best characterized by independent parameters. The two length scales are the total convective length of the flame experienced by a disturbance during convection through the flow field, and the HRR weighted center of mass of the flame heat release region measured from the source location of convected disturbances. These length scales appropriately nondimensionalize the magnitude and the phase, respectively. A sketch of these length scales is shown in Fig. 2. What this implies for the two types of flames discussed here is that for both attached (HSI) and lifted (LSI) flames, regardless of the origin of the perturbations, the flame length (from base to tip) should be the governing parameter for the magnitude. Further, given that the phase should be governed by convection from the disturbance origin to the center of mass, identifying the actual disturbance origin for lifted flames will be critical in order to achieve accurate normalizations and scaling.

In the present study we compare flame transfer function measurements for both HSI, and the less-studied LSI flames, both subject to EGR conditions. The explicit goal of this approach is to identify the impact of EGR (simulated by diluent addition) on the combustion dynamics in both of these flame geometries. Also, diluent addition has been shown previously to provide an additional 'knob' for control of the flame structure semi-independently from other operating conditions [9], [10]. As such, this represents a potentially useful basis for attempts at further generalization of flame transfer function measurements.

III. Experimental Setup

Experimental studies of flame dynamics were carried out for traditionally swirl stabilized (HSI) and low-swirl injector (LSI) stabilized flames. Regarding this nomenclature, LSI refers to a specific type of stabilizer design (reported by Cheng et. al. [11]), and is not simply descriptive of the degree of swirl. The traditional swirl-stabilized geometry, while possessing a higher geometric swirl number than the LSI, is principally termed HSI in this study for contrast, as other differences in the configurations exist that will be subsequently detailed.

The experimental apparatus used in this study was configured slightly differently for HSI and LSI measurements. Generally speaking, the rig was a straight (21.6mm inner diameter) tube nozzle that lead into a rapid expansion. Combustion occured at the expansion (dump plane), which was enclosed by a 79 mm diameter quartz tube for optical access. The quartz tube had a length of 203mm, considered a 'short' configuration to prevent self-excited instabilities from developing for any of the conditions studied. A sketch of the apparatus in the low-swirl injector configuration is shown in Fig. 3. While the term 'injector' is used to describe both configurations, fuel, air and diluent were actually well-mixed

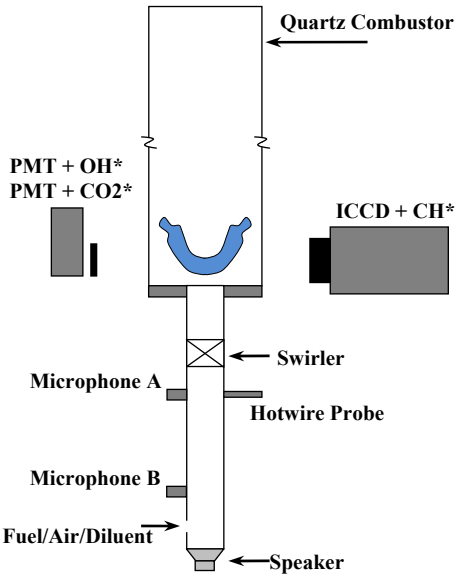

Fig. 3 – Sketch of the rig configured for LSI flame FRF measurements. Approximate locations of diagnostics shown.

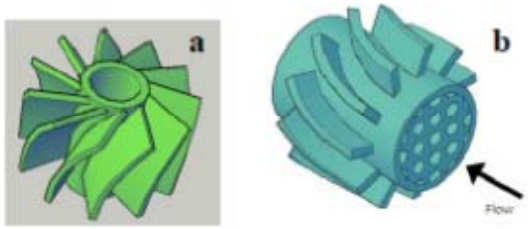

Fig. 4a and b - CAD drawing of the high and low-swirl injectors used in this study. The arrow on the LSI indicates the flow direction.

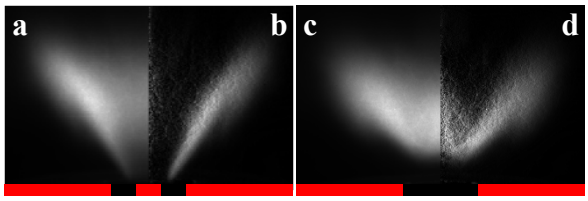

Fig. 5 – a) Time-averaged image of HSI flame at Q = 100 lpm, Φ = 0.80; b) Abel inversion of previous; c) Time-averaged image of LSI flame at Q = 100 lpm, Φ = 0.80; d) Abel inversion of previous

upstream of the nozzle in both cases. Additionally, a choke plate was placed between the mixing location and the nozzle to prevent any acoustic oscillations from causing variations in the reactant mixture. Fuel, air and diluent concentrations were all metered using a set of mass flow controllers. Fuel for all cases in this study was methane. Different levels of EGR were simulated by introducing varying levels of N_2 and CO_2. Dilution levels are reported as a percentage of the total volumetric flow rate. In the case of N_2 dilution, the reported dilution level refers only to the additional nitrogen added, excluding the nitrogen already present in the air.

The high- and low-swirl injectors refer to a set of static swirl vanes that were placed within the rig at locations of 38mm and 29.5mm upstream of the dump plane, respectively. The LSI design was similar to that investigated by Cheng et. al. [11]. The HSI had a geometric swirl number of around 0.88 while the LSI's value was around 0.5. The swirler configurations also differed in that the HSI used an 8.8mm diameter centerbody which extended through the center of the swirler to the dump plane, while the LSI featured an open central grid that produces an unswirled core flow. Solid models of the swirlers are shown in Fig. 4, highlighting the latter difference. Due to the difference in use of a centerbody, while the high-swirl injector produced a V-shaped flame which attached directly on the centerbody, the low-swirl injector flame was aerodynamically stabilized and as a result was lifted from the dump plane. Sample images of the two flame types are shown in Fig. 5.

Transfer functions were measured by introducing a velocity excitation using a speaker mounted at the base of the nozzle (shown in Fig. 3). The excitation amplitude was maintained such that velocity excitations (in the nozzle directly upstream of the swirler) had amplitude less than approximately 15% of the mean, which has been reported as a suitable threshold for linear behaviors [19]. The linearity of the measurements was further tested by varying the excitation amplitude around the baseline level and ensuring the invariance of the measured transfer function. Excitations were introduced one frequency at a time over the range of 50-500 Hz with a 10Hz interval. This sine-dwell approach was used to provide strong coherence between the input and output. The low frequency limit of 50Hz was imposed by loss of transfer function coherence. The velocity excitation was measured using a hotwire anemometer inserted into the flow upstream of the swirler (see Fig. 3). The heat release rate (HRR) response of the

flame was measured via global measurements of the OH* chemiluminescence [32] made by a photomultiplier tube filtered at 308nm. Additionally, spatially resolved images of the unexcited flame CH* chemiluminescence were obtained using an intensified CCD camera averaging 25 images, each acquired with a 5ms gate, to provide images of the steady flame HRR distribution.

The flame convective length scales were obtained from these line-of-sight steady flame images at each particular operating condition. The flame regions within the images were first obtained by thresholding using the MATLAB built-in GRAYTHRESH routine, which automatically calculates suitable thresholding levels using a method derived from Otsu [33]. The flame length was measured using the axial extrema of this region, that is, the axial distance between the first and last pixels within the binarized image. For the purposes of flame length calculation, the HSI flames were assumed to always be attached at the dump plane, while the base edge of the LSI flame was allowed to float (consider L_f in the sketch in Fig. 2). The flame center of mass was calculated by computing the center of mass of the axial HRR distribution, weighted by local HRR intensity, accounting only for pixels within the thresholded flame region. In both HSI and LSI configurations, the origin for the disturbances was assumed to be the dump plane. This implies that the physical representation modeled by this nondimensionalization was based on convective disturbances (an example would be vortices) which were shed at the dump plane and convected axially through the flame. The convective velocity scale used was the mean velocity (flow rate divided by area) in the nozzle for the appropriate swirl configuration, accounting for the centerbody area when applicable.

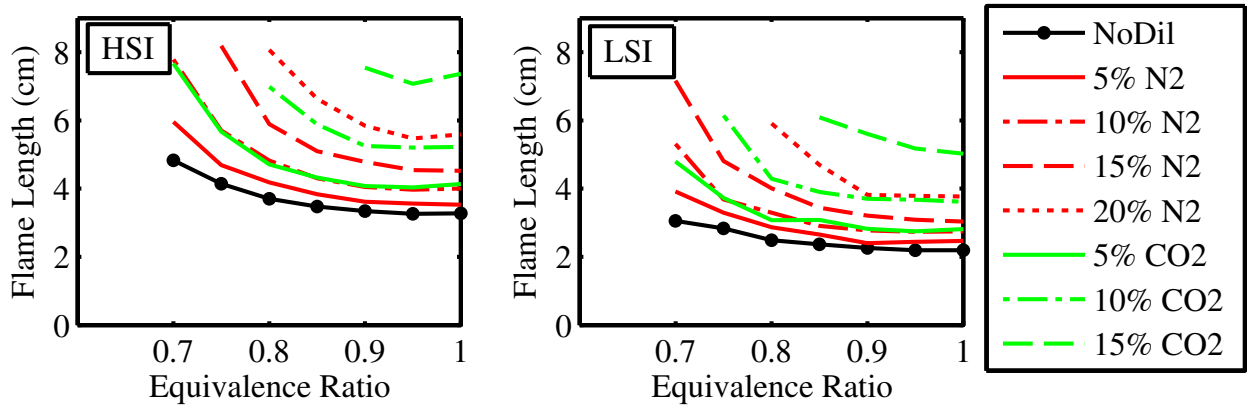

Fig. 6 – Flame lengths for HSI and LSI flames measured at varying dilution and equivalence ratio conditions. All data shown is for a total flow rate of 100 LPM.

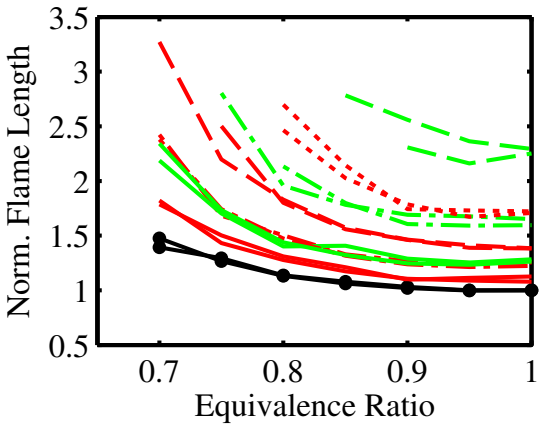

Fig. 7 – Comparison of normalized flame lengths for both injector types. Flow rate of 100LPM. Legend is the same as in Fig. 6.

IV. Results and Discussion

A. Steady flame characteristics

The flame length was measured for both LSI and HSI flames, with results shown in Fig. 6. Flame lengths increase with decreasing equivalence ratio, increasing dilution and (not shown) increasing flow rate. These results match trends what would be anticipated based on the expected relationship between these operating conditions and flame speed. LSI flames were found to be shorter overall than HSI flames at equivalent operating conditions. Generally speaking, CO_2 was observed to have a larger affect on the flame length than an equal quantity of N_2. One explanation for this observation may be the higher specific heat of CO_2, meaning heating of CO_2 diluent requires more energy from the flame and may be expected to cause a larger effect on the flame speed. Notably, for both swirler types, the case of 10% dilution with N_2 produced flames with similar lengths as dilution by 5% CO_2. Additionally, the absolute variation in flame length observed for LSI flames was less than their HSI counterparts. However, the relative variation was comparable for each type of flame (as normalized to the shortest flame at equivalence ratio of 1.0 with no dilution), as shown in Fig. 7. This behavior is similar for variation with respect to flow rate as well. The importance of this proportionality is best observed in

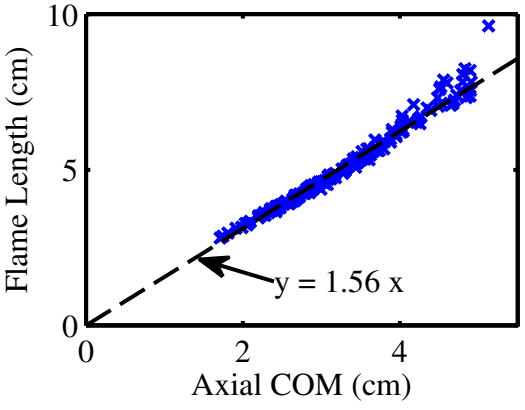

Fig. 8 – Flame length and center of mass are proportional. Points show data for all test conditions for the HSI.

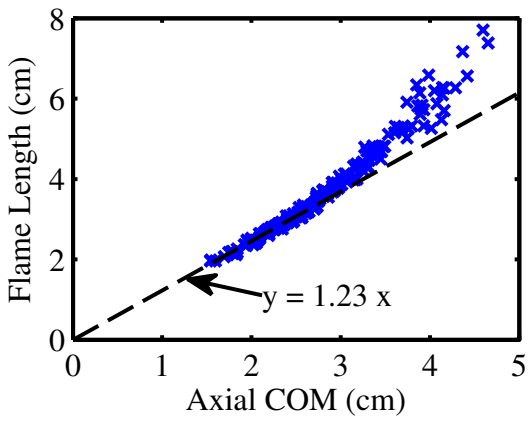

Fig. 9 – Flame length and center of mass are proportional for short flames. Points show data for all test conditions for the LSI.

considering Eq. 2, which suggests that for a given percent change in the characteristic length, an equivalently proportional change in frequency is induced. Thus, according to Fig. 7, when making changes to operating condition, the critical frequencies should exhibit the same percentage variation regardless of injector type. The successful normalization of the data with respect to Strouhal number detailed in subsequent sections confirms this expectation.

The proportionality between flame length and flame center of mass previously reported in literature for HSI type flames [14] was also observed here, as shown in Fig. 8. As stated, this proportionality implies that using either center of mass or flame length as the characteristic length should each produce similarly effective scaling of the flame transfer function dynamics, but prevents differentiating between the two as to the actual governing physical basis for the dynamics. Considering the same comparison for the LSI flames, in Fig. 9, this proportionality still exists for short flames, but begins to deviate somewhat with lengthening flames. This indicates that as overall flame length increases for an LSI, the center of mass remains somewhat preferential to the dump plane. This effect is primarily due to non-linearity in the liftoff distance. In other words, the flame length from the base edge to the tip remains approximately proportional to the distance from the flame base to the center of mass, while liftoff distance varies. Even with the deviation in long LSI flames, the approximate proportionality that exists for both injector types in this study obstructs differentiation of the physical governing length scale based on observations made from normalization.

B. Transfer Functions

Flame transfer functions for each swirl configuration were measured as a function of various operating conditions. The transfer functions for both the LSI and HSI exhibited similar characteristics, as shown in Fig. 10. The magnitude exhibited a low-pass filter characteristic, decreasing with increasing frequency (i.e. Strouhal number). In many cases, a 'notch' was observed in the magnitude, occurring around a Strouhal number of 0.5 for the LSI and around 0.75 for the HSI case. Despite the decreasing magnitude associated with this notch, all cases maintained strong transfer function coherence (extremes >0.8, with typical values >0.95), indicating continued correlation between the input an output at these frequencies. The HSI exhibited some significant variation in the overall shape of the magnitude transfer function, with the severity of the notch feature increasing with increasing equivalence ratio. This effect was not observed in the LSI, which we attribute to the fact that the overall flame

length variation for the tested operating conditions was less in the LSI case. The notch has been attributed in the literature either to spatially occurring interference between the up- and down-stream halves of the flame [13] which can be further attributed to the occurrence of multiple perturbations that produce an interference-like response [13], [23]. Both cases exhibited greater variability in the occurrence of higher frequency dynamics occurring beyond this first interference-like feature.

For both LSI and HSI geometries, phase was dominated by delay. Rapid shifts in the phase occur coincident with 'notch' behaviors in the magnitude. Considering Fig. 11a, the rapidity of the phase shift appears to exhibit correspondence with the severity of the notch feature. Uniquely, in the case of the LSI, these rapid shifts in the

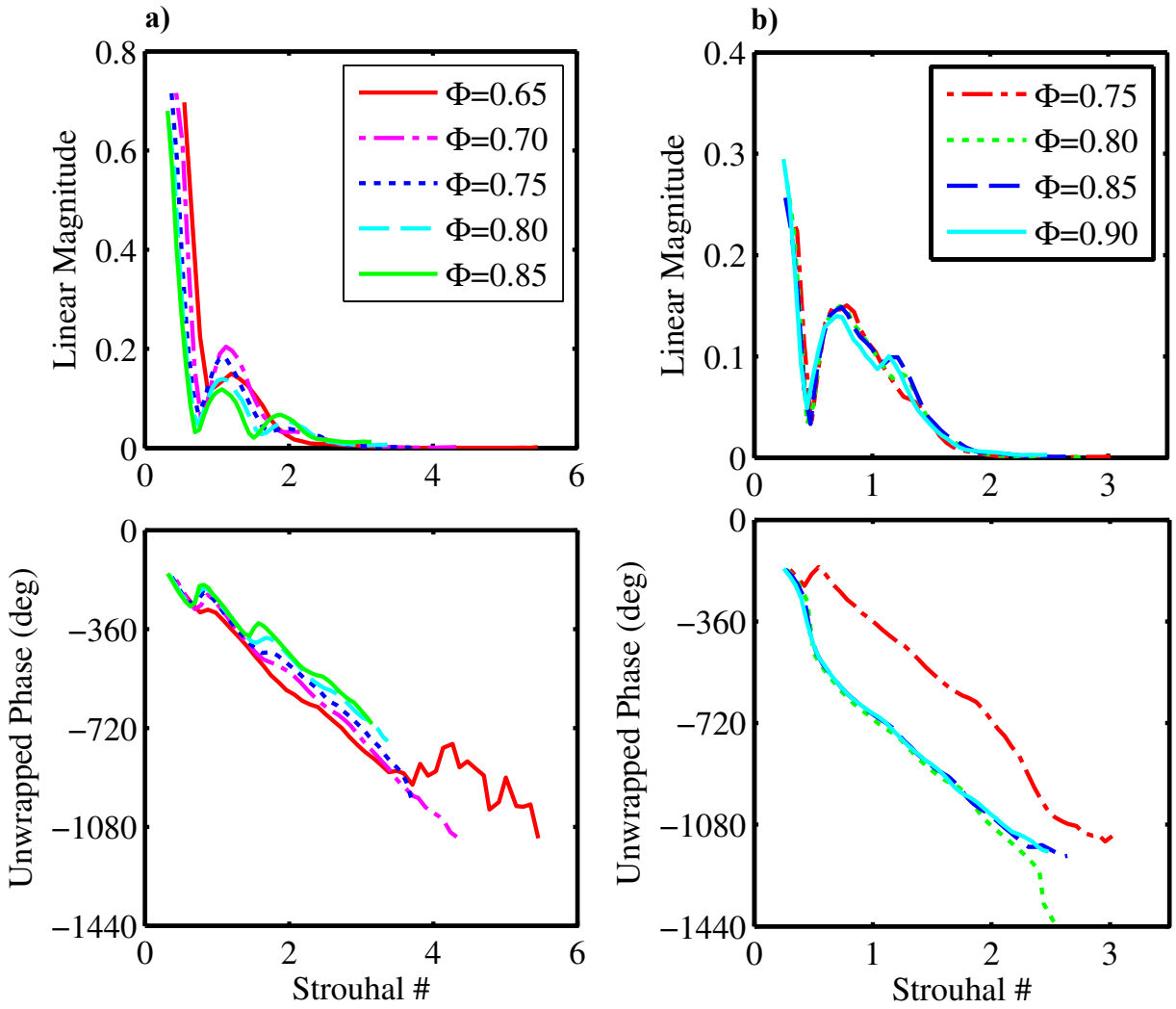

Fig. 10 – Flame transfer functions for a)HSI and b) LSI with respect to variation in equivalence ratio. Mean flow rate for all cases shown is 100 SLPM, with pure methane as fuel. All Strouhal numbers use flame length and average velocity in the nozzle for scaling.

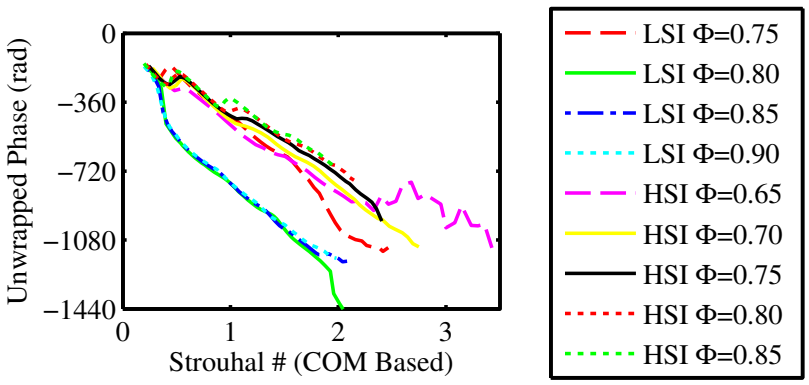

Fig. 11 – Phase as a function of Strouhal number based on flame center of mass position. Both LSI and HSI shown. All cases are for undiluted methane at flow of 100 SLPM.

phase occured in both positive and negative directions. Modeling efforts [29] suggest that the direction of the phase shift may be associated with the relative shapes of heat release rate distributions relative to the nature of disturbances that lead to the heat release rate response. According to the same modeling efforts, the low frequency phase slope (e.g. prior to any dynamic effects) has the most ability to indicate the convective velocity. Using a Strouhal number based on the center of mass for each case produces the plot shown in Fig. 11. The mean slope determined by the low frequency phase corresponds in this case to a delay 1.7 times greater than that corresponding to the mean velocity (i.e. a convective velocity of 0.59 times the mean nozzle velocity). Durox et. al., studying laminar inverted conical flames, specifically relate this delay to interaction with convected vortices at half the maximum flow velocity [18]. This is also similar to the convective velocity of 60% of the mean nozzle velocity reported by Jones et al. [23]. The fact that center of mass normalization produced the same velocity for both injector types suggests that convected disturbances arise for both injection geometries at the dump plane and interact throughout the flame. Thus, inclusion of the liftoff distance in the center of mass calculation is necessary for LSI flames when determining the transfer function phase, consistent with the model [29].

C. Effect of flow rate

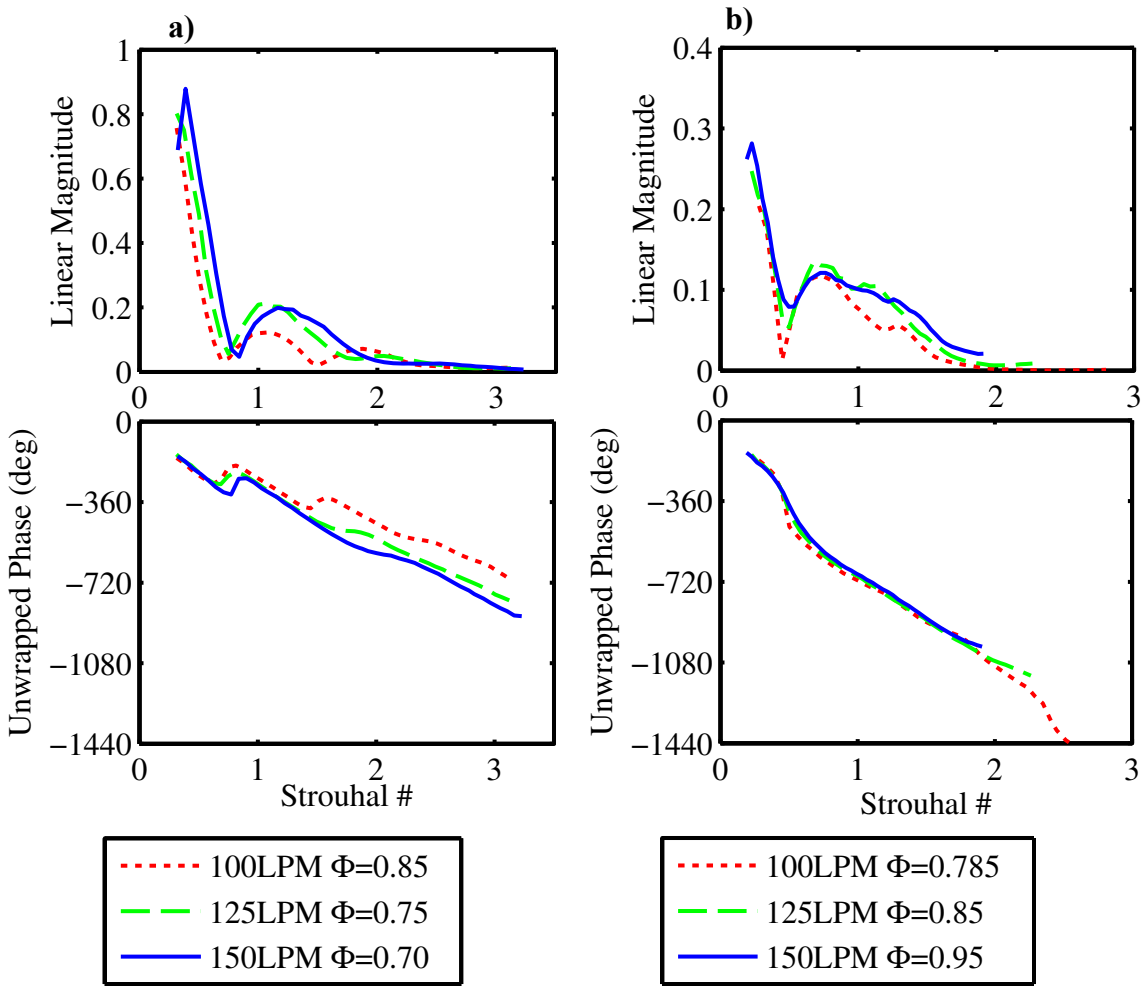

Fig. 12 – Flame transfer functions subject to varying flow rates for a)HSI and b) LSI. Fuel for all cases was pure methane with no dilution. All Strouhal numbers use flame length and average velocity in the nozzle for scaling.

Flow rate variations were tested in a similar fashion to the equivalence ratio variation results. Several conditions of total flow rate from 100-150 LPM were considered. Results are shown in Fig. 12. Fundamentally, the response is similar to that discussed previously. As with the equivalence ratio variations, flow rate variations produce some changes to the flame transfer function characteristics, expecially beyond the occurrence of the first notch feeature. For both injector types, increasing the fuel flow rate produced some damping effect on the severity of the notch. This effect was greater on the LSI injector as compared to the HSI. The same phase delay for each case was still observed relative to the Strouhal number scaling, indicating that even for variable mean flow velocity, the convective velocity remains around 59% of the mean nozzle velocity for both injector geometries.

D. Effects of dilution

Similar analysis may be conducted to consider the effect of EGR, simulated by dilution, on the flame transfer function. Several cases were tested maintaining an approximately fixed flame length. Compared to a baseline case without any dilution, it can be seen from Fig. 13 that dilution essentially has no effect on the transfer function characteristics for a fixed flame length. This implies that the dilution had no unique dynamic impact on the flame transfer function for either type of injector. Changes in flame length associated with dilution would be expected to alter the response in a similar way to the variations in equivalence ratio discussed in the preceding section. This provides an explanation for the results of Ferguson et. al. [9], [10], who observed that the influence of EGR on instabilities in a combustor could be characterized using only convective scaling laws. For a fixed flame length,

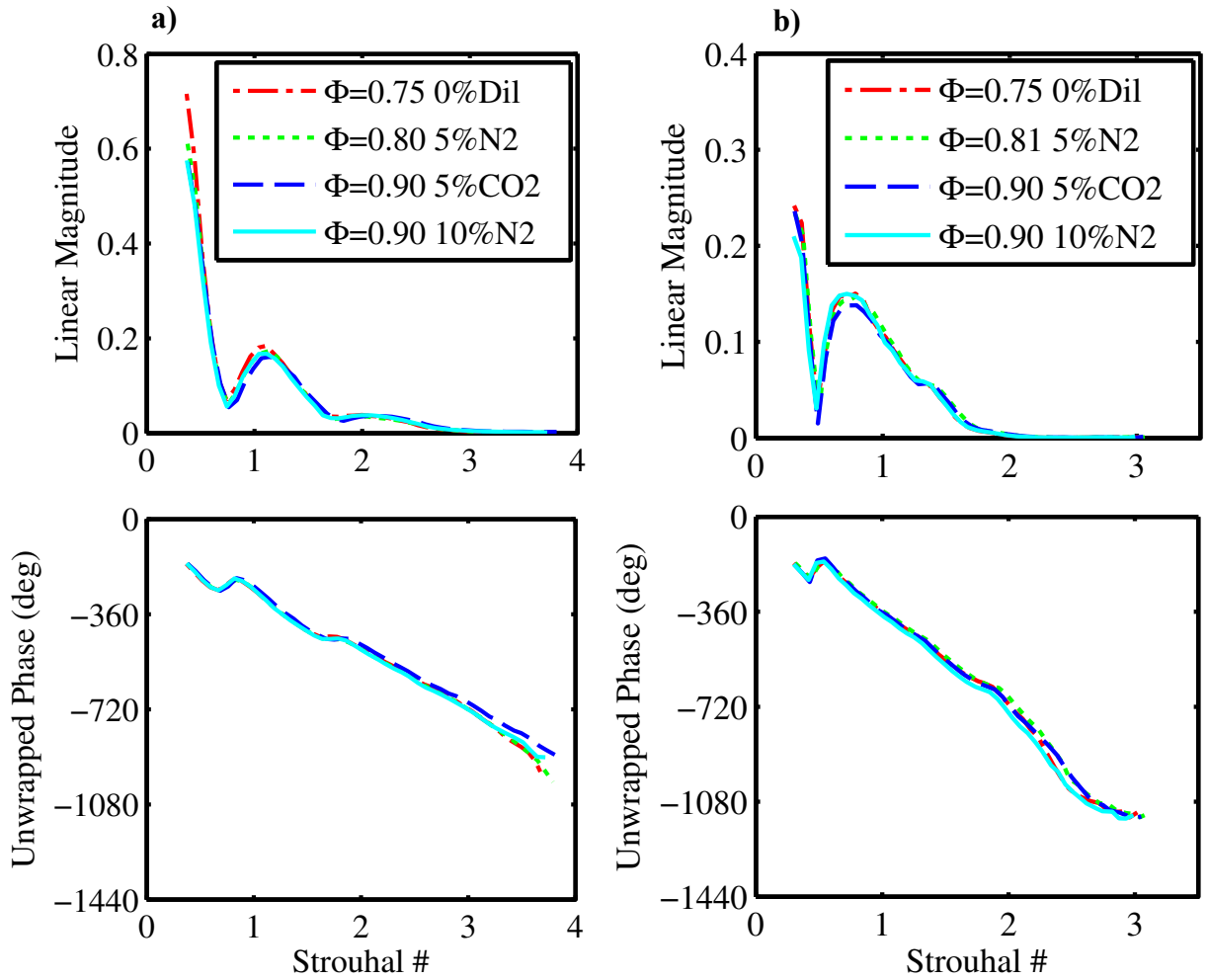

Fig. 13 – Flame transfer functions subject to varying levels of dilution for a)HSI and b) LSI. Mean flow rate for all cases shown is 100 SLPM. Dilution levels are reported as a percentage of the total volumetric flow. All Strouhal numbers use flame length and average velocity in the nozzle for scaling.

modest levels of dilution did not alter the flame transfer function, and thus would not be expected to influence the instability behaviors of the combustor.

While the characteristics of transfer function itself were unaltered by the addition of dilution, one aspect not addressed by the normalized transfer function is that of the transfer function gain. By definition, so long as the flame consumes all the delivered fuel, the transfer function has a DC gain value with respect to velocity disturbances of unity (i.e. steady heat release rate is directly proportional to mass flow rate of fuel for lean combustion). Thus, without normalization, DC gain is theoretically equal to the ratio between steady heat release rate and velocity. In the absence of diluent, the only gain variation with respect to operating condition should therefore come with changes in equivalence ratio. Introduction of variations in diluent level introduce an additional, different dependence of the gain on operating condition. The theoretical DC gain (assuming lean flames and complete combustion) obeys the following relationship:

$$DC\ Gain = \frac{\bar{Q}}{\bar{u}} = \left(\rho_{fuel} A_{nozzle} LHV_{fuel}\right) \frac{1 - \%dil}{1 + \frac{A/F)_{s,vol}}{\Phi}} \qquad (3)$$

Increasing diluent, like decreasing the equivalence ratio, causes a decrease in the theoretical DC gain. However, the fact that the dependence on these two operating condition parameters are not the same provides a mechanism by which the length and the DC gain can vary semi-independently as shown in Fig. 14. Ferguson and Ranalli [34] also report the possibility of varying the flame temperature independently of the flame length. So the presence of dilution provides an additional 'knob' on the operating condition that allows for independence of DC gain, characteristic length and flame temperature. This leads to the possibility of analyzing the effects of these parameters independently and may in a general sense motivate the use of diluent to provide additional experimental control in future flame dynamics studies. In addition, novel dynamic control strategies may be available through the use of diluent, where a constant flame temperature can be maintained while lengthening the flame to create a deliberate change in the characteristic frequencies of the flame transfer function.

E. Interference Effects

To further investigate the occurrence of the 'notch' in the transfer functions, several measurements were made of phase locked images of the flame subject to acoustic excitation, following analysis by Palies et. al. [13]. Images of the flame were acquired at an interval of 36 degrees over an entire cycle. At each phase, 500 images taken with a

100μs gate were averaged to produce the oscillating flame response. The axial heat release profile was measured from the raw intensities of these images, and the flame was split in half at 50% of the cumulative axial heat release, as shown in Fig. 15. The integrated heat release (intensity) from each of the axial half-images was then plotted over a cycle and compared with the global value, shown in Fig. 16.

The frequencies shown in Fig. 16 correspond to the location of the first magnitude notch and the first rebound peak from the notch for each of the injectors considered. Due to the different responses of the injectors, these occur at different frequencies. The frequencies for the HSI are 110Hz and 160Hz for the notch and rebound respectively. For the LSI, they are 90Hz and 140Hz. It is clearly evident from the graphs that in the notch feature, the two halves of the flame can be said to oscillate out of phase for both injectors, in agreement with Palies et. al. [13]. This provides a possible mechanism for the occurrence of the notch; due to the convective nature of the disturbances, a single disturbance creates a spatial interference pattern resulting in nearly complete destructive interference. Thus, the global response of the flame (measured in the transfer function) is suppressed, producing a decrease in magnitude. The response behavior at the first rebound is varies somewhat between the two injectors. While in both cases the halves of the flame are closer to being in-phase than at the notch, the downstream half of the HSI flame exhibits an observable lag from the upstream half. The LSI occurs nearly in phase for this case. According to the physics predicted by physical representation of the Strouhal number approach [29], pure axial convection for a constant intensity flame should result in flame halves which are approximately 90 degrees out of phase at the first

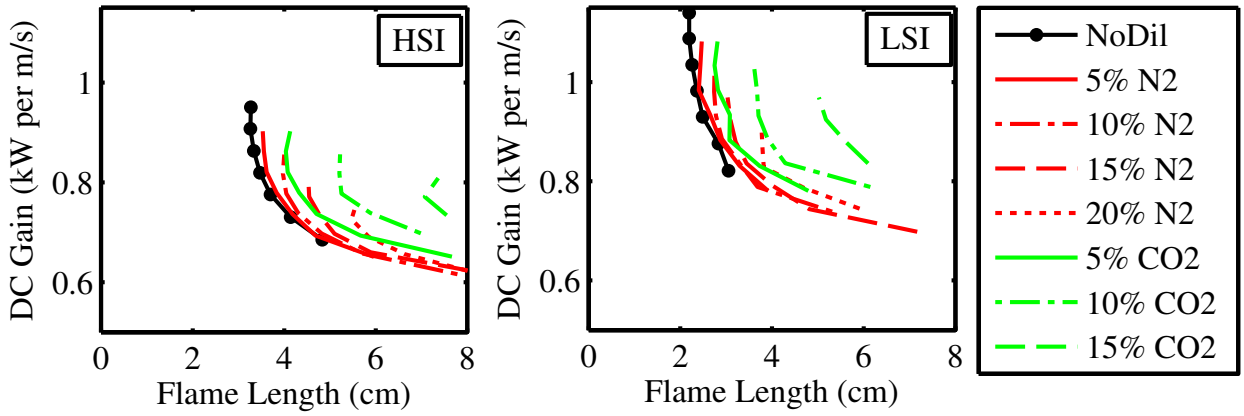

Fig. 14 – DC Gain vs. Flame Length computed for varying dilution and equivalence ratio conditions. All data shown is for a total flow rate of 100 LPM. Notably, gain and length can be changed independently with introduction of dilution.

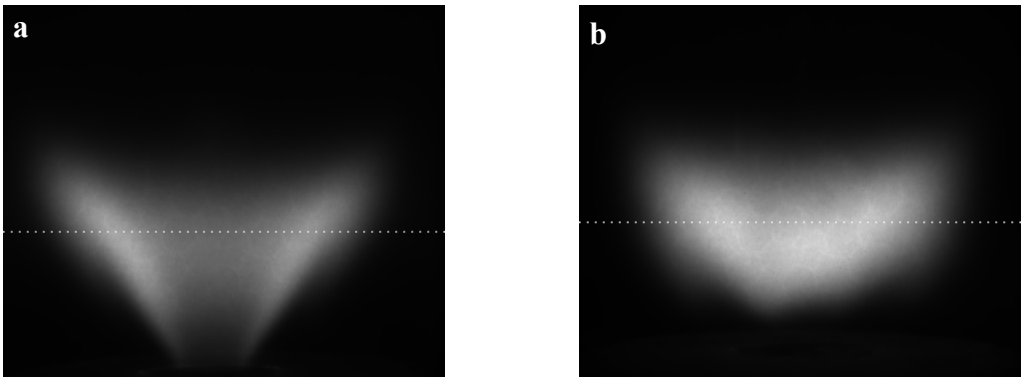

Fig. 15 – Steady images averaged over the entire cycle, showing the axial 50-50 split location for the intensity. a) HSI, b) LSI

rebound peak, with the upstream half lagging. This prediction at the rebound frequency differs somewhat from the observed results in Fig. 16. As stated in the background, several different mechanisms involving the occurrence of multiple perturbations, have been suggested for the occurrence of this phenomenon, including swirl disturbances, vortical disturbances and simple acoustic interactions. Definite conclusions about the nature of the disturbances leading to the measured phase relationships are not possible from the data herein. Nonetheless, it is sufficiently clear that the for both injector geometries, phase between spatially independent portions of the flame is relevant to the character of the global transfer function.

In addition to tracking the somewhat holistic behavior of the intensity, it is also possible to track the evolution of the phase throughout the image, as in Fig. 17. Phase maps were obtained by calculating the phase of every image pixel over the cycle of excitation. They are shown in for each flame at the same frequencies as previously. These plots provide an extremely interesting visualization of the transport of disturbances throughout the flow field. The HSI predominantly experiences streaks of falling phase overlapping with the steady flame surface. The LSI on the other hand exhibits a greater incidence of radial delay indicating that the disturbances move both downstream and outward through the flame simultaneously. More sophisticated analysis that makes use of flow field data to analyze the delay relative to actual local velocity could represent a possible avenue for continued study.

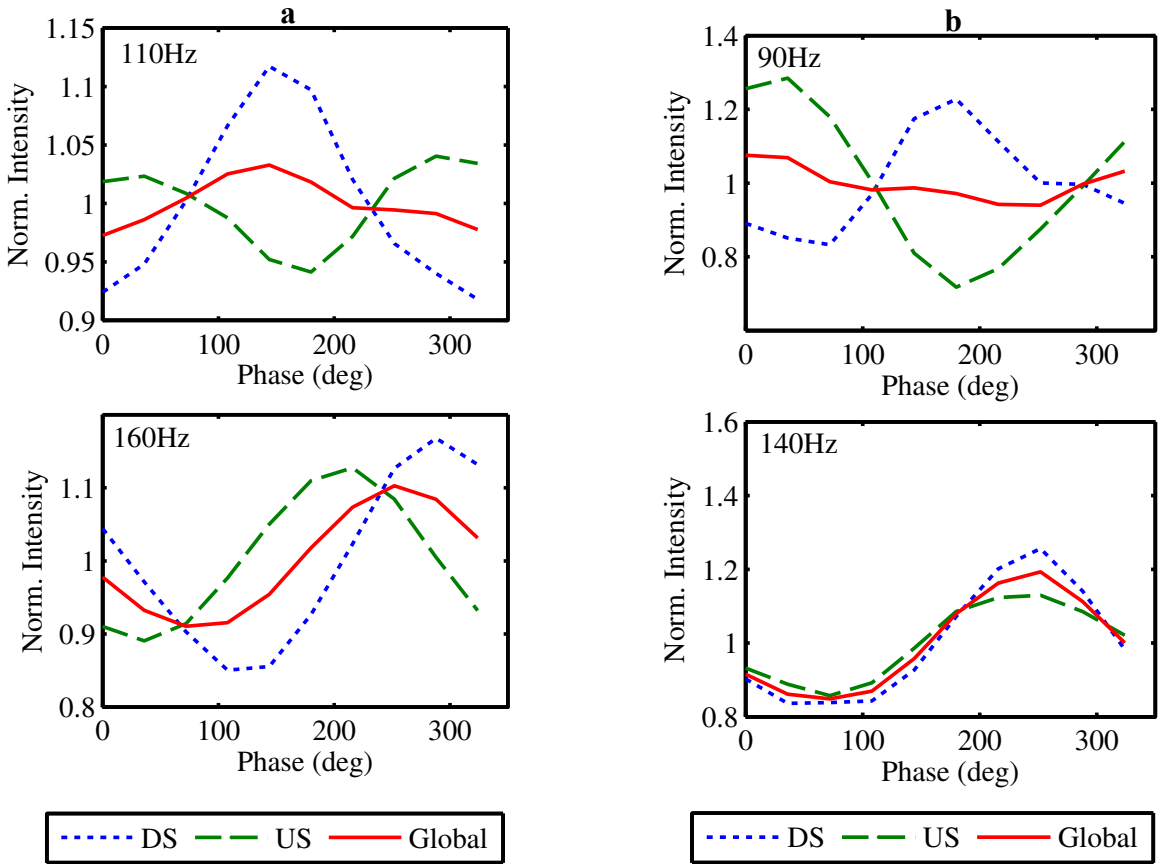

Fig. 16 – Amplitude of oscillation of the flame split axially into upstream (US) and downstream(DS) halves. Left: HSI 100 LPM, Phi = 0.80, No diluent at frequencies 110Hz and 160Hz. Right: LSI 100LPM, Phi = 0.90, no diluent at frequencies 90Hz and 140Hz. Frequencies correspond to the first notch and the first rebound peak after the notch for their respective transfer functions.

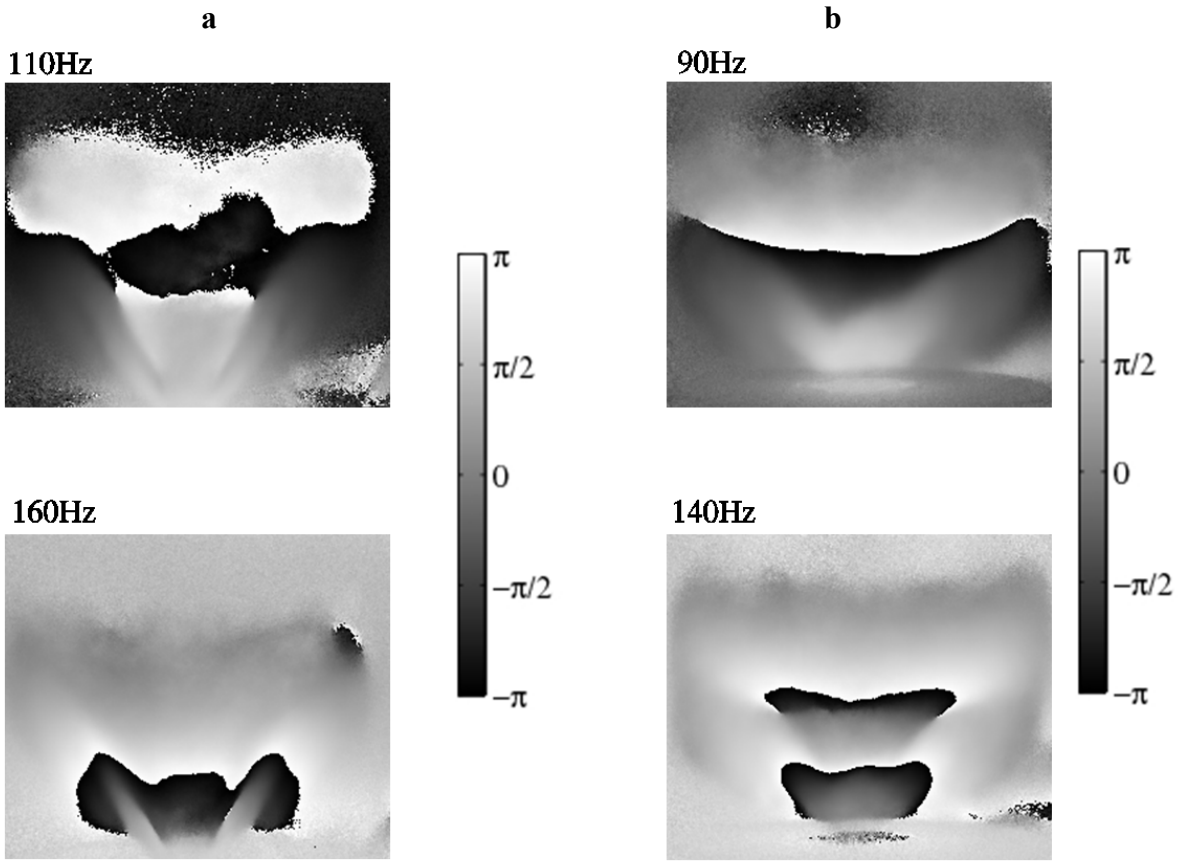

Fig. 17 – Line-of-sight image based phase maps for Left: HSI and Right: LSI at the same pairs of frequencies as Fig. 16. Scale ranges from pi to –pi in radians. Note that sharp edges may exhibit simple wrapping of the phase from –pi to pi, rather than actual rapid changes in the phase.

V. Conclusions

Flame transfer functions play a useful role in analysis of the coupling mechanisms leading to thermoacoustic instabilities. Flame transfer function measurements were made for two flame stabilization geometries and with the addition of N_2 and CO_2 dilution, simulating the effect of exhaust gas recirculation. Both the low-swirl and high-swirl injectors produced flame transfer functions that were substantially similar. Flame transfer functions measured in this study exhibited similar behaviors to those reported in literature, including low-pass filter characteristics and evidence of destructive interference effects in the magnitude. The transfer function phase was dominated by convective delay.

Analysis of the transfer function subject to variations in several different operating conditions showed similar results to the baseline case. Normalization by Strouhal number produced transfer functions for which the occurrence

of the primary interference feature remained approximately invariant for a fixed injector. However, the notch occurred at different Strouhal numbers between the two injectors, taking values of around 0.75 and 0.5 for the HSI and LSI, respectively. Higher frequency dynamics showed greater variability with respect to changes in equivalence ratio and flow rate. Convective scaling was analyzed using the measured low-frequency delay in the flame transfer function phase, resulting in identical calculated convective velocity values for both injectors of around 0.59 times the mean velocity.

Further analysis of the apparent destructive interference observed in the transfer function magnitude was conducted using phase locked images of the flame subject to the acoustic forcing. It was observed that the incidence of the destructive interference 'notch' corresponded to a case in which the two axial halves of the flame produced out-of-phase chemiluminescence intensity (thus, HRR) oscillations. Both types of injector considered in this study exhibited this behavior. This observation is consistent with the hypothesis that the interference is producecd as a result of spatially distributed disturbances with variable spatial phase due to their convective nature.

For a fixed flame length, modest changes in the level of dilution were shown to have no affect on the transfer function. This is especially significant for applications utilizing EGR for carbon capture indicating that even in the presence of EGR, existing scaling laws for combustion dynamics would be expected to apply, albeit subject to an additional parameter governing the flame size. Flames subject to both equivalence ratio and dilution level variations produce gains (and flame temperatures) which are somewhat independent from variation in flame length. As such use of both dilution and equivalence ratio as parametric controls provides an additional degree of experimental control, unavailable with either alone. This may also merit further investigation as an additional avenue for deliberate control of instabilities in practical systems that utilize EGR.

Acknowledgement

The support of the U.S. DOE Turbines program is gratefully acknowledged. J. Ranalli gratefully acknowledges the support of the Oak Ridge Institute for Science and Education (ORISE) Postdoctoral Fellowship program.

Refereces

[1] T. Griffin, D. Bucker, and A. Pfeffer, "Technology options for gas turbine power generation with reduced CO2 emission," *JOURNAL OF ENGINEERING FOR GAS TURBINES AND POWER-TRANSACTIONS OF THE*, vol. 130, no. 4, Jul. 2008.

[2] C. Botero, M. Finkenrath, M. Bartlett, R. Chu, G. Choi, and D. Chinn, "Redesign, Optimization, and Economic Evaluation of a Natural Gas Combined Cycle with the Best Integrated Technology CO2 Capture," *Energy Procedia*, vol. 1, no. 1, pp. 3835–3842, Feb. 2009.

[3] O. Bolland and P. Mathieu, "Comparison of two CO2 removal options in combined cycle power plants," *Energy Conversion and Management*, vol. 39, no. 16–18, pp. 1653–1663, Dec. 1998.

[4] S. Hoffmann, M. Bartlett, M. Finkenrath, A. Evulet, and T. Ursin, "Performance and Cost Analysis of Advanced Gas Turbine Cycles With Precombustion CO2 Capture," *Journal of Engineering for Gas Turbines and Power*, vol. 131, no. 2, Mar. 2009.

[5] A. M. ElKady, A. Evulet, A. Brand, T. P. Ursin, and A. Lynghjem, "Exhaust Gas Recirculation in DLN F-Class Gas Turbines for Post-Combustion CO2 Capture," *ASME Conference Proceedings*, vol. 2008, no. 43130, pp. 847–854, 2008.

[6] A. T. Evulet, A. M. ELKady, A. R. Branda, and D. Chinn, "On the Performance and Operability of GE's Dry Low NOx Combustors utilizing Exhaust Gas Recirculation for PostCombustion Carbon Capture," *Energy Procedia*, vol. 1, no. 1, pp. 3809–3816, Feb. 2009.

[7] P. Rokke and J. Hustad, "Exhaust Gas Recirculation in Gas Turbines for Reduction of CO2 Emissions; Combustion Testing with Focus on Stability and Emissions," *Internationa Journal of Thermodynamics*, vol. 8, no. 4, pp. 167–173, Dec. 2005.

[8] H. Li, A. M. ElKady, and A. T. Evulet, "Effect of Exhaust Gas Recirculation on NOx Formation in Premixed Combustion System," in *47th AIAA Aerospace Sciences Meeting*, Orlando, FL, 2009, vol. AIAA-2009-226.

[9] D. Ferguson, J. Ranalli, and P. Strakey, "INFLUENCE OF EXHAUST GAS RECIRCULATION ON COMBUSTION INSTABILITIES IN CH4 AND H2/CH4 FUEL MIXTURES," in *Proceedings of the ASME Turbo Expo*, Glasgow, UK, 2010, vol. GT2010-23642.

[10] D. Ferguson and J. Ranalli, "Characterization of Instabilities in a Low-Swirl Injector with Exhaust Gas Recirculation," in *49th AIAA Aerospace Sciences Meeting including the New Horizons Forum and Aerospace Exposition*, Orlando, FL, 2011, vol. AIAA-2011-517.

[11] R. K. Cheng, D. Littlejohn, P. A. Strakey, and T. Sidwell, "Laboratory investigations of a low-swirl injector with H2 and CH4 at gas turbine conditions," *Proceedings of the Combustion Institute*, vol. 32, no. 2, pp. 3001–3009, 2009.

[12] S. Ducruix, D. Durox, and S. Candel, "Theoretical and experimental determinations of the transfer function of a laminar premixed flame," *Proceedings of the Combustion Institute*, vol. 28, no. 1, pp. 765–773, 2000.

[13] P. Palies, D. Durox, T. Schuller, and S. Candel, "The combined dynamics of swirler and turbulent premixed swirling flames," *Combustion and Flame*, vol. 157, no. 9, pp. 1698–1717, Sep. 2010.

[14] M. Lohrmann and H. Buchner, "Prediction of stability limits for LP and LPP gas turbine combustors," *Combustion Science and Technology*, vol. 177, no. 12, pp. 2243–2273, Dec. 2005.

[15] D. Kim and S. W. Park, "Effects of hydrogen addition on flame structure and forced flame response to velocity modulation in a turbulent lean premixed combustor," *Fuel*, vol. 89, no. 11, pp. 3475–3481, Nov. 2010.

[16] J. Ranalli, C. Martin, P. Black, U. Vandsburger, and R. West, "Measurement of Flame Transfer Functions in Swirl-Stabilized, Lean-Premixed Combustion," *Journal of Propulsion and Power*, vol. 25, no. 6, pp. 1350–1354, Dec. 2009.

[17] J. Ranalli and D. Ferguson, "Measurement of Flame Frequency Response Functions in a Low-Swirl Flame under Exhaust Gas Recirculation Conditions," in *49th AIAA Aerospace Sciences Meeting including the New Horizons Forum and Aerospace Exposition*, Orlando, FL, 2011, vol. AIAA-2011-518.

[18] D. Durox, T. Schuller, and S. Candel, "Combustion dynamics of inverted conical flames," *Proceedings of the Combustion Institute*, vol. 30, no. 2, pp. 1717–1724, Jan. 2005.

[19] R. Balachandran, B. O. Ayoola, C. F. Kaminski, A. P. Dowling, and E. Mastorakos, "Experimental investigation of the nonlinear response of turbulent premixed flames to imposed inlet velocity oscillations," *Combustion and Flame*, vol. 143, no. 1–2, pp. 37–55, Oct. 2005.

[20] K. T. Kim, J. G. Lee, B. D. Quay, and D. A. Santavicca, "Spatially distributed flame transfer functions for predicting combustion dynamics in lean premixed gas turbine combustors," *Combustion and Flame*, vol. 157, no. 9, pp. 1718–1730, Sep. 2010.

[21] C. Külsheimer and H. Büchner, "Combustion dynamics of turbulent swirling flames," *Combustion and Flame*, vol. 131, no. 1–2, pp. 70–84, Oct. 2002.

[22] S. Shanbhogue, D. Shin, S. Hemchandra, D. Plaks, and T. Lieuwen, "Flame sheet dynamics of bluff-body stabilized flames during longitudinal acoustic forcing," *Proceedings of the Combustion Institute*, vol. 32, pp. 1787–1794, 2009.

[23] B. Jones, J. G. Lee, B. D. Quay, and D. A. Santavicca, "Flame Response Mechanisms Due to Velocity Perturbations in a Lean Premixed Gas Turbine Combustor," *J. Eng. Gas Turbines Power*, vol. 133, no. 2, p. 021503–9, Feb. 2011.

[24] J. O'Connor and T. Lieuwen, "Further Characterization of the Disturbance Field in a Transversely Excited Swirl-Stabilized Flame," *Journal of Engineering for Gas Turbines and Power*, vol. 134, no. 1, p. 011501, 2012.

[25] P. Palies, T. Schuller, D. Durox, and S. Candel, "Modeling of premixed swirling flames transfer functions," *Proceedings of the Combustion Institute*, vol. 33, no. 2, pp. 2967–2974, 2011.

[26] Preetham, H. Santosh, and T. Lieuwen, "Dynamics of Laminar Premixed Flames Forced by Harmonic Velocity Disturbances," *Journal of Propulsion and Power*, vol. 24, no. 6, pp. 1390–1402, Dec. 2008.

[27] T. Schuller, D. Durox, and S. Candel, "A unified model for the prediction of laminar flame transfer functions: comparisons between conical and V-flame dynamics," *Combustion and Flame*, vol. 134, no. 1–2, pp. 21–34, Jul. 2003.

[28] D. You, Y. Huang, and V. Yang, "A generalized model of acoustic response of turbulent premixed flame and its application to gas-turbine combustion instability analysis," *Combustion Science and Technology*, vol. 177, no. 5–6, pp. 1109–1150, Jun. 2005.

[29] J. Ranalli, D. Ferguson, and C. Martin, "Simple analysis of flame dynamics via flexible convected disturbance models," *Journal of Propulsion and Power*, vol. Submitted Aug 2011.

[30] V. Acharya, Shreekrishna, D.-H. Shin, and T. Lieuwen, "Swirl effects on harmonically excited, premixed flame kinematics," *Combustion and Flame*, vol. 159, no. 3, pp. 1139–1150, Mar. 2012.

[31] D. M. Kang, F. E. C. Culick, and A. Ratner, "Combustion dynamics of a low-swirl combustor," *Combustion and Flame*, vol. 151, no. 3, pp. 412–425, Nov. 2007.

[32] J. Lee and D. Santavicca, "Experimental diagnostics for the study of combustion instabilities in lean premixed combustors," *Journal of Propulsion and Power*, vol. 19, no. 5, pp. 735–750, Oct. 2003.

[33] N. Otsu, "A threshold selection method from gray-level histograms," *IEEE Transactions on Systems, Man and Cybernetics*, vol. 9, no. 1, pp. 62–66, Jan. 1979.

[34] D. Ferguson and J. Ranalli, "Utilization of Exhaust Gas Recirculation for Control of Dynamic Combustion Instabilities," presented at the 7th US National Technical Meeting of the Combustion Institute, Atlanta, GA, 2011.